Hydrodynamic performance of a hybrid anaerobic baffled reactor (HABR): effects of number of chambers, hydraulic retention time, and influent temperature

Md Khalekuzzaman, Mehedi Hasan, Rezaul Haque and Muhammed Alamgir

ABSTRACT

Hydrodynamic performance of a biological reactor is an important design concern since it directly affects the treatment efficiency. In this research, a hybrid anaerobic baffled reactor (HABR) was proposed with improved design concepts and principles. The HABR consisted of a front sedimentation chamber, four regular baffled chambers followed by two floated filter media chambers. The effects of operating variables 5–20 hr hydraulic retention time (HRT) and 10–40 °C of influent temperature, as well as their interactive effects, on the hydrodynamic behaviour were investigated by residence time distributions study and response surface methodology. The study suggests that the hydrodynamic performance is greatly influenced by the number of chambers in the reactor rather than HRT and influent temperature. The influence of HRT and feed temperature were mainly observed on the front chambers (1–4) rather than rear chambers (5–7). The optimum reactor performance – low dead space (<10%), excellent hydraulic efficiency (>0.75), and intermediate mixing pattern (Peclet number > 10) – were achieved using the proposed HABR with more than five chambers.

Key words | hybrid anaerobic baffled reactor, hydraulic retention time, hydrodynamic performance, influent temperature, residence time distribution

Md Khalekuzzaman (corresponding author)
Mehedi Hasan
Rezaul Haque
Muhammed Alamgir
Department of Civil Engineering,
Khulna University of Engineering & Technology (KUET),
Khulna,
Bangladesh
E-mail: *kzaman.ce.kuet@gmail.com*

INTRODUCTION

Over the last few decades, attention has been given to anaerobic biological wastewater treatment owing to its advantages of energy saving, biogas recovery, and lower sludge production (Liew Abdullah *et al.* 2005; Feng *et al.* 2009). One of the most efficient high-rate anaerobic reactor is the anaerobic baffled reactor (ABR) developed by McCarty and co-workers at Stanford University. Conceptually, the ABR may be represented as a series of up-flow anaerobic sludge blanket reactors, one of the most popular anaerobic treatment systems (Li *et al.* 2015).

The ABR, which belongs to the third-generation high-rate anaerobic reactors, is highly appraised for its high efficiency, outstanding working stability, and lower operating cost (Xu *et al.* 2014). The advantages of this bioreactor include low maintenance requirements, rapid biodegradation, low yields of sludge, and excellent process stability. This configuration is an effective solution to the treatment of wastewater for most small and medium-sized plants which possess little economic capacity to invest in environmental controls (Chan *et al.* 2009). The major drawback of the ABR is that there have been very few full-scale ABR applications for wastewater treatment until now. In addition, when comparing with the traditional aerobic process, anaerobic treatment system processes poor effluent quality, which usually needs post-treatment to meet the discharge limits. Further research on advanced reactor design and control process could lead to most of the ABR's disadvantages being overcome. Perhaps, the ABR may be one of the solutions answering the global call for low-maintenance, robust treatment systems (Reynaud & Buckley 2016).

ABR process characteristics and its hydraulic characteristics are closely related. The hydraulic rather than the organic loading rate is a treatment limiting factor for ABR

doi: 10.2166/wst.2018.379

systems (Reynaud & Buckley 2016). The conversion of organic and inorganic matter in an anaerobic treatment process is governed by two interrelated factors: the reactor's hydrodynamics, which are predominantly affected by its configuration, and the performance of the microbiological processes (Qi *et al.* 2013). The strong interdependence of hydraulics and kinetics means that the hydraulic performance directly affects the pollutant removal performance (Persson *et al.* 1999; Li *et al.* 2015). Hence, the hydrodynamic behaviour of a biological reactor is one of the fundamental factors for its wastewater treatment efficiency. The hydrodynamics and degree of mixing that occur within a biological reactor strongly influence the extent of contact between the substrate and bacteria, thus controlling mass transfer. Unfavourable hydraulic conditions in the bioreactor may cause lower system performance, and thus resulting higher residual concentrations in the treated effluent. Thus, mixing mode and intensity of mixing are the two important factors for good reactor configuration for efficient treatment (Renuka *et al.* 2016).

In addition, influent temperature has a significant effect on the reactor treatment efficiency. Researchers (Nachaiyasit & Stuckey 1997; Feng *et al.* 2008; Wu *et al.* 2016) have shown that treatment efficiencies of the ABR changed with temperature variations. Similar findings have been reported in their studies that there was no or low effect on treatment efficiency when operated at 25–35 °C, but the reactor efficiency deteriorated significantly when the temperature dropped below 15 °C. However, there is no information available on the effect of influent temperature on hydrodynamic performance especially on dead space, mixing pattern, and hydraulic efficiency that ultimately affect the reactor treatment performance.

The tracer test is a proven method for determining the residence time distribution (RTD), defined as the time-varying distribution of a particle entering and leaving the system. Therefore, RTD curves obtained from tracer tests can be employed to analyse the flow patterns (Xu *et al.* 2014). RTD curves can then be incorporated into the 'dispersion model' and 'tank-in-series model' (Levenspiel 1999). Thus, the model calculates the dead space (unused volume), dispersion (degree of mixing), short circuiting and hydraulic efficiency.

Although much research has been conducted on the hydraulic characteristics of ABRs (Grobicki & Stuckey 1992; Liu *et al.* 2007; Sarathai *et al.* 2010; Ji *et al.* 2012; Xu *et al.* 2014; Li *et al.* 2015, 2016; Sharma & Kazmi 2015; Renuka *et al.* 2016), few studies have been carried out on the effects of influent temperature at variable hydraulic retention time (HRT) on the hydrodynamic performance of the reactor. The present study aims to determine the hydraulic behaviour of the hybrid anaerobic baffled reactor (HABR) under different influent temperatures (10–40 °C) and HRTs (5–20 hr) through RTD study, and to evaluate their interactive effects by response surface methodology (RSM). The main aim of the study was to develop a HABR with optimum reactor performance which would minimize dead space, maximize hydraulic efficiency, and improve mixing pattern of the reactor.

MATERIALS AND METHODS

Experimental set-up

Reactor configuration

The schematic diagram of the HABR is shown in Figure 1. The reactor used in this study was constructed with acrylic

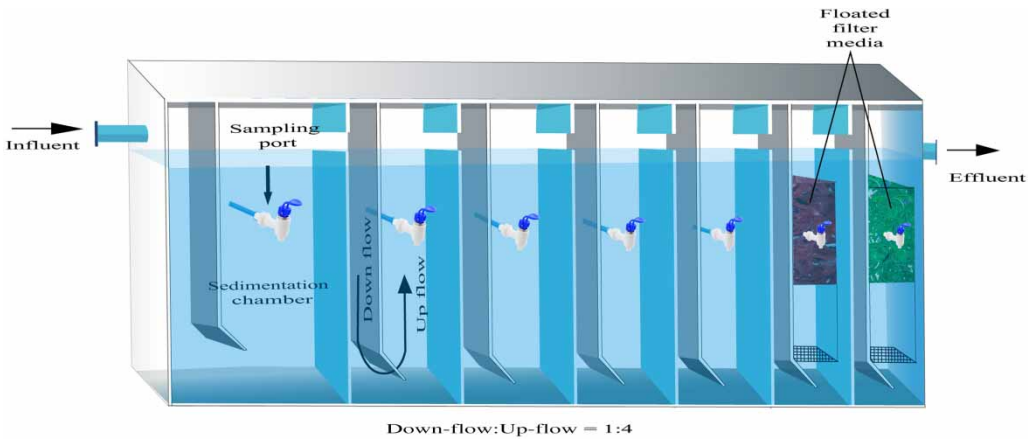

Figure 1 | Schematic of the hybrid anaerobic baffled reactor.

sheet, with external dimensions of 90, 20, and 30 cm for length, width, and depth, respectively. The HABR consisted of a front sedimentation chamber and four regular chambers followed by two floated filter media chambers. The first chamber volume, designed as a settling chamber, was twice that of the subsequent chambers. The effective volume of the reactor was 36.4 L. The individual chambers were divided into two portions by a hanging baffle, which separated each chamber into a down- and up-flow zone. The ratio between down-flow and up-flow was 1:4, and the bottom portion of the baffle was inclined at 45°. Each chamber had a sampling port located at 20 cm from the base on the front side of the reactor. Approximately 400 g of shredded soft drink lids were loosely placed as floated filter media in the last two chambers of the reactor. These locally available materials were used due to their favourable physical properties that would not allow reactor failure through clogging during wastewater treatment. The summary of the HABR configuration is presented in Table 1.

Table 1 | Summary of HABR configuration

Design parameter	Specification
ABR dimensions	90 cm (L) × 20 cm (W) × 30 cm (H)
Effective volume	36.4 L
First chamber/settler	2 V (V is volume of subsequent chamber)
Deflector angle of hanging baffle	45°
Down-flow:up-flow	1:4
Type of filter media	Floated filter media (shredded soft drink lids, density – 109 kg/m^3, specific gravity – 0.93) (grinding of soft drink lids)
Sampling port	20 cm (from base) at center
Inlet/outlet	Inlet: 27 cm from base; outlet: 25 cm from base

Flow pattern

Nine experimental runs were conducted to investigate the hydraulic characteristics of the HABR obtained from RTD analyses (Table 2). Experimental runs A (A1, A2, and A3), B (B1, B2, and B3) and C (C1, C2, and C3) were conducted using a peristaltic pump (WT600-1F, Longer Pump Co., China) fed with tap water for 5, 10, and 20 hr HRT, respectively. A NUVE BM30 water bath was used to maintain influent temperature (10, 25, and 40 °C) during each HRT run. The feeding system was operated by a Sino-timer which was programmed to run for 10 min/hr during the experiment. All experiments were conducted between 21 °C and 25 °C room temperature.

Table 2 | Summary of different experimental runs (A1 to C3)

Run No.	HRT (hr)	Pump run time (min/hr)	Pump flow rate (mL/min)	Influent temp. (°C)
A1	5	10	181.90	10 ± 5
A2	5	10	181.90	25 ± 5
A3	5	10	181.90	40 ± 5
B1	10	10	363.80	10 ± 5
B2	10	10	363.80	25 ± 5
B3	10	10	363.80	40 ± 5
C1	20	10	727.60	10 ± 5
C2	20	10	727.60	25 ± 5
C3	20	10	727.60	40 ± 5

Tracer experiment

Tracer studies were performed by stimulus–response technology. Sodium chloride (NaCl) was selected as the tracer due to its various favourable features as described by Li *et al.* (2015, 2016). To obtain the RTD curves, 200 mL concentrated NaCl solution (42.5 g Cl^-/Cl) was instantaneously injected prior to the inlet. The water samples were collected from the sampling port of each chamber and the effluent of the reactor at regularly spaced intervals from the time of impulse ($t = 0$), and the total sampling time was 2.5 times the nominal HRT. The sampling frequency was 0.125 times of HRT except for 0.06 times of HRT between 0.6 HRT and 1 HRT during each tracer experiment run. The chloride ion (Cl^-) concentration was measured using a conductivity meter (Model CD-4302, Lutron, Taiwan) after calibrating with standard conductivity solution (Model CD-14, 1.413 mS) (Levenspiel 1999; Sharma & Kazmi 2015), and the Cl^- concentration of tap water was also subtracted from each sample in RTD calculation for all runs.

Theoretical interpretation

RTD and dead space

The RTD was investigated by tracer stimulus–response technology. To compare the mixing patterns of different runs, the unit of time is normalized:

$$\theta = \frac{t}{HRT} \quad (1)$$

where θ is the normalized time (dimensionless), t is the sampling time, and HRT is the theoretical hydraulic retention time.

$$C_\theta = \frac{C(t)}{C_0} \tag{2}$$

where C_θ is the normalized tracer concentration at dimensionless time θ, $C(t)$ is the tracer concentration at time t, and C_0 is the initial tracer concentration.

Equations (1) and (2) provide the normalized concentration C_θ and normalized time θ values to be plotted along vertical vs horizontal axis for the RTD study. The normalized curve is also known as E-curve (exit age curve). The most important characteristic of the E-curve is that the area under the curve is equal to 1 as defined in Equation (3)

$$\int_0^\infty E(t)dt = 1 \tag{3}$$

where $E(t)$ is the RTD function. The $E(t)$ value is related to the $C(t)$ value as shown in Equation (4), which was used to calculate the mean residence time ($\bar{t}$) and distribution variance (σ_t^2), Equation (5).

$$E(t) = \frac{C(t)}{\int_0^\infty C(t)dt}$$

$$\bar{t} = \frac{\int_0^\infty tC(t)dt}{\int_0^\infty C(t)dt} = \int_0^\infty tE(t)dt \tag{4}$$

$$\sigma_t^2 = \frac{\int_0^\infty (t-\bar{t})^2 C(t)dt}{\int_0^\infty C(t)dt} = \int_0^\infty t^2 E(t)dt - (\bar{t})^2 \tag{5}$$

The dead space (V_d, %) is calculated using Equation (6) as explained by Ji *et al.* (2012) and Li *et al.* (2016):

$$V_d = \left(1 - \frac{\bar{t}}{HRT}\right) \times 100\% \tag{6}$$

Short circuiting

Metcalf & Eddy (2003) explained short circuiting as a complicated phenomenon that influences reactor performance. It is considered as one of the greatest hindrances for the success of a reactor (Tsai *et al.* 2012). Short circuiting (ψ) can be expressed as the ratio of the first appearance of tracer (t_f) in the effluent to the theoretical HRT (HRT) as shown in Equation (7).

$$\psi = \frac{t_f}{HRT} \tag{7}$$

The short-circuiting value of 0.3 or less indicates a flow with significant short circuiting (Sarathai *et al.* 2010).

Axial dispersion model

In case of relatively low back-mixing, the axial dispersion (AD) model can be applied (Ji *et al.* 2012). It is assumed that the back-mixing only occurs in the axial direction as expressed by the dispersion coefficient. The mixing in the radial direction is neglected in the AD model. In addition, it is assumed that the fluid possesses a constant velocity and constant substrate concentration across the bed diameter (Renuka *et al.* 2016). Under steady-state condition, the governing equation for mass balance is established by applying Fick's law as follows in Equation (8):

$$\frac{\partial C}{\partial t} = D\frac{\partial^2 C}{\partial x^2} - u\frac{\partial C}{\partial x} \tag{8}$$

where D is the axial dispersion coefficient, m^2/sec; t is the time, sec; x is the axial distance of the reactor, m; and u is the average fluid velocity in the flow direction, m/sec. A dimensionless form of Equation (8) can be expressed as Equation (9):

$$\frac{\partial C}{\partial \theta} = \left(\frac{D}{uL}\right)\frac{\partial^2 C}{\partial Z^2} - \frac{\partial C}{\partial Z} = D_d\frac{\partial^2 C}{\partial Z^2} - \frac{\partial C}{\partial Z} \tag{9}$$

where D_d represents dispersion number (D_d=D/uL); C=$C(t)/C_0$, L is length of the reactor, and Z=$(ut+x)/L$. The dimensionless dispersion number specifies the extent of axial dispersion in the reactor. A large dispersion number (D_d=∞) implies a perfectly mixed system, whereas a small dispersion number (D_d=0) relates to a plug-flow system. Similarly, D_d=0.02 is defined as intermediate, and D_d=0.2 is as a large degree of dispersion (Renuka *et al.* 2016).

In order to solve Equation (9), it is required to mention the boundary condition of the reactor. For a closed-vessel boundary condition, in which only axial mixing is considered, Equation (10) is used to obtain normalized variance as a function of dispersion number (Levenspiel 1999).

$$\sigma_\theta^2 = 2\left(\frac{D}{uL}\right) - 2\left(\frac{D}{uL}\right)^2 (1 - e^{-(uL/D)}) \tag{10}$$

where σ_θ^2 is the dimensionless variance of RTD, $\sigma_\theta^2 = (\sigma_t^2/(\bar{t})^2)$.

Alternatively, Peclet number Pe is often used to express the mixing pattern, which is just the reciprocal of the dispersion number ($Pe = (uL/D)$) as expressed by Equation (11).

$$\sigma_\theta^2 = \left(\frac{2}{Pe}\right) - 2\left(\frac{1}{Pe}\right)^2 (1 - e^{-Pe}) \tag{11}$$

The large value of Pe means weaker back-mixing (Li *et al.* 2016). From the above equations, it can be noted that the dead space calculation is associated with the mean of the curve, while the dispersion or Peclet number is associated with the variance of the curve (Liu *et al.* 2007).

Tank-in-series model

In the case of relatively strong back-mixing, the tank-in-series (TIS) model is applied as suggested by Grobicki & Stuckey (1992) by Equation (12):

$$C(t) = \frac{C_0}{(N-1)!}(t/\tau)^{(N-1)} e^{-t/\tau} \tag{12}$$

where τ is the theoretical HRT and N is the number of TIS.

$$\sigma_\theta^2 = \int_0^\infty \frac{N^N \theta^{N+1} e^{-N\theta}}{(N-1)!} d\theta - 1 = \frac{1}{N} \tag{13}$$

Equation (13) can be used to calculate the dimensionless variance of TIS, and N can be calculated by Equation (14) below.

$$N = \frac{1}{\sigma_\theta^2} \tag{14}$$

If N tends to 1, the flow pattern of the reactor approaches that of a continuous stirred tank reactor (CSTR). On the other hand, when N tends to ∞, the flow pattern approaches a plug flow.

Hydraulic efficiency

The hydraulic efficiency (λ) includes two basic features: (i) the distribution of flow across the reactor and (ii) the mixing of reaction liquid (Ji *et al.* 2012). It is dependent on the effective volume (e) and the flow pattern as expressed in Equation (15):

$$\lambda = e\left(1 - \frac{1}{N}\right) \tag{15}$$

The effective volume is calculated by subtracting the value of dead space from 1. The hydraulic efficiency of the system can be classified into three categories: (1) excellent hydraulic efficiency with $\lambda > 0.75$, (2) good hydraulic efficiency with $0.5 < \lambda \leq 0.75$, and (3) poor hydraulic efficiency with $\lambda \leq 0.5$.

RESULTS AND DISCUSSION

The normalized concentrations of Cl^- for all samples, collected at the sampling port of each chamber and the effluent, were plotted against normalized time for different runs A1 to C3 (Figure 2). The RTD results are summarized in Table 3. Figures 3, 4(a), 4(b), and 5 show the dead space, dispersion number, TIS, and hydraulic efficiency, respectively, for all chambers and effluent sample for all runs.

Residence time distribution

The normalized concentrations of chloride ion Cl^- for all seven chambers and effluent were plotted against normalized time for different runs A1 to C3 (Figure 2). As shown in the figure, the RTD curve firstly rose and then dropped, forming one single peak for all chambers except the first chamber, which behaved as a CSTR. There were minor effects observed on the RTD curve for the different runs (A1 to C3) with 5 hr to 20 hr HRT, and 10 °C to 40 °C of influent temperature; however, the RTD curves significantly differed between the chambers. This indicates that the reactor hydrodynamic behaviour was primarily influenced by number of chambers of the reactor than by operating parameters (e.g. HRTs and/or influent temperature). Further analyses of the RTD curve showed that the peak normalized concentration (C_θ) gradually decreased from 2.01 ± 0.28 for chamber 1 to 0.81 ± 0.17 for effluent. The peak C_θ appeared at $\theta = 0.1$ for chamber 1 and then gradually decreased at $\theta = 1$ for effluent. This represents higher reactor dead space for chamber 1, which then gradually decreased for subsequent chambers. The results indicated similar finding as Thackston *et al.* (1987) and Sarathai *et al.* (2010)

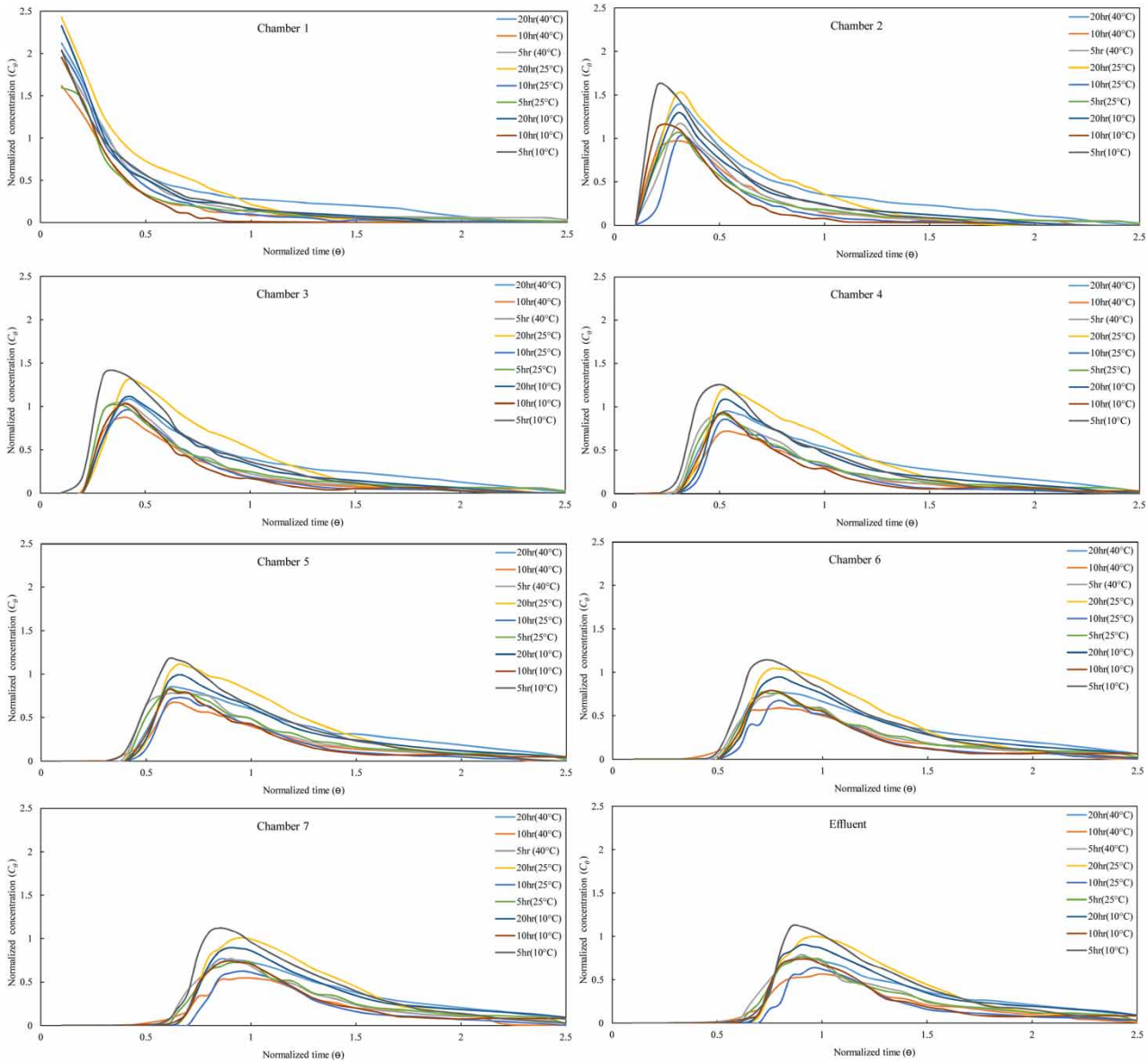

Figure 2 | Residence time distribution curves of chambers (1–effluent) for different experimental runs (A1 (5 hr–10 °C), A2 (5 hr–25 °C), A3 (5 hr–40 °C), B1 (10 hr–10 °C), B2 (10 hr–25 °C), B3 (10 hr–40 °C), C1 (20 hr–10 °C), C2 (20 hr–25 °C), C3 (20 hr–40 °C)).

reported; further the peak C_θ curve moves towards the left from $\theta = 1$, which indicates increasing of dead space.

Dead space and short circuiting

Dead space in the reactor can be generally divided into hydraulic dead space and biological dead space. Hydraulic dead space is a function of the flow rate and the number of compartments in the ABR, and the biological dead space is a function of the biomass concentration and activity (Grobicki & Stuckey 1992). The present study examined the effects of different HRTs – 5, 10, and 20 hr – at different influent temperatures of 10, 25, and 40 °C on hydraulic dead space. The hydraulic dead space is the major contributor to dead space in the ABR system (Sarathai *et al.* 2010). The results showed deviation of the actual HRT ($\bar{t}$, hr) from the theoretical HRT for all runs (A1 to C3), which indicated the presence of dead space and/or short circuiting within the reactor as presented in Table 3. The dead space calculated from RTD curve for different runs A1 to C3 are also shown in Figure 3. The results showed that the dead space for all runs reduced to zero between chamber 4 and 6.

Table 3 | Results of RTD studies

Run	Chamber	$\bar{t}$ (hr)	V_d (%)	D/uL	N	λ	Ψ	Run	Chamber	$\bar{t}$ (hr)	V_d (%)	D/uL	N	λ	Ψ	Run	Chamber	$\bar{t}$ (hr)	V_d (%)	D/uL	N	λ	Ψ
A1	ch-1	1.9	61.6	1.33	1.3	0.08	0.1	**A2**	ch-1	2.3	54.1	∞	0.9	0.00	0.1	**A3**	ch-1	2.4	52.3	∞	0.9	0.00	0.1
	ch-2	2.8	44.8	0.28	2.5	0.33	0.2		ch-2	3.4	31.2	0.50	1.8	0.30	0.2		ch-2	3.3	33.0	0.52	1.7	0.28	0.1
	ch-3	3.3	34.4	0.19	3.2	0.45	0.2		ch-3	3.8	23.5	0.31	2.3	0.43	0.3		ch-3	3.7	25.1	0.33	2.2	0.41	0.2
	ch-4	4.0	19.5	0.13	4.4	0.62	0.3		ch-4	4.6	8.3	0.17	3.5	0.66	0.4		ch-4	4.4	11.6	0.18	3.4	0.62	0.3
	ch-5	4.8	4.1	0.09	5.9	0.80	0.4		ch-5	5.0	–	0.12	4.7	0.79	0.5		ch-5	5.0	0.7	0.13	4.5	0.77	0.4
	ch-6	5.0	–	0.07	7.3	0.86	0.5		ch-6	5.0	–	0.09	6.2	0.84	0.6		ch-6	5.0	–	0.09	6.3	0.84	0.5
	ch-7	5.0	–	0.06	9.6	0.90	0.6		ch-7	5.0	–	0.07	8.1	0.88	0.7		ch-7	5.0	–	0.07	8.1	0.88	0.6
	Effluent	5.0	–	0.05	10.5	0.91	0.6		Effluent	5.0	–	0.07	8.2	0.88	0.7		Effluent	5.0	–	0.07	8.1	0.88	0.6
B1	ch-1	2.4	76.2	0.43	1.9	0.11	0.1	**B2**	ch-1	3.4	65.6	∞	1.0	0.00	0.1	**B3**	ch-1	4.2	58.4	∞	0.9	0.00	0.1
	ch-2	4.7	53.1	0.32	2.3	0.26	0.2		ch-2	5.8	41.5	0.30	2.3	0.33	0.2		ch-2	6.2	38.2	0.40	2.0	0.31	0.1
	ch-3	6.5	34.9	0.24	2.7	0.41	0.3		ch-3	6.7	33.2	0.19	3.2	0.46	0.3		ch-3	7.4	26.4	0.27	2.5	0.44	0.2
	ch-4	8.4	15.7	0.17	3.5	0.60	0.4		ch-4	8.3	17.0	0.11	5.2	0.67	0.4		ch-4	9.0	9.6	0.15	4.0	0.68	0.3
	ch-5	9.8	1.6	0.12	4.8	0.78	0.5		ch-5	9.7	2.6	0.08	6.7	0.83	0.5		ch-5	10.0	–	0.10	5.6	0.82	0.4
	ch-6	10.0	–	0.09	6.2	0.84	0.6		ch-6	10.0	–	0.07	8.0	0.88	0.6		ch-6	10.0	–	0.08	7.1	0.86	0.5
	ch-7	10.0	–	0.07	8.2	0.88	0.7		ch-7	10.0	–	0.05	11.2	0.91	0.8		ch-7	10.0	–	0.05	10.3	0.90	0.5
	Effluent	10.0	–	0.06	8.3	0.88	0.7		Effluent	10.0	–	0.05	10.6	0.91	0.8		Effluent	10.0	–	0.06	9.5	0.89	0.6
C1	ch-1	7.6	61.8	4.30	1.1	0.03	0.1	**C2**	ch-1	7.6	62.0	0.74	1.5	0.13	0.1	**C3**	ch-1	11.1	44.6	2.77	1.1	0.06	0.1
	ch-2	12.8	35.9	0.30	2.3	0.37	0.2		ch-2	11.8	40.8	0.18	3.4	0.42	0.2		ch-2	15.5	22.5	0.33	2.2	0.42	0.2
	ch-3	15.4	23.1	0.19	3.2	0.53	0.3		ch-3	14.9	25.6	0.13	4.4	0.57	0.3		ch-3	17.9	10.4	0.21	3.0	0.60	0.3
	ch-4	18.7	6.7	0.13	4.3	0.72	0.4		ch-4	17.4	12.8	0.09	5.9	0.72	0.4		ch-4	20.0	–	0.14	4.2	0.76	0.4
	ch-5	20.0	–	0.10	5.6	0.82	0.5		ch-5	20.0	–	0.07	7.4	0.87	0.5		ch-5	20.0	–	0.10	5.4	0.81	0.5
	ch-6	20.0	–	0.08	7.1	0.86	0.6		ch-6	20.0	–	0.06	8.9	0.89	0.6		ch-6	20.0	–	0.08	6.8	0.85	0.6
	ch-7	20.0	–	0.06	8.8	0.89	0.7		ch-7	20.0	–	0.05	11.3	0.91	0.7		ch-7	20.0	–	0.06	9.0	0.89	0.7
	Effluent	20.0	–	0.06	8.9	0.89	0.7		Effluent	20.0	–	0.04	11.9	0.92	0.7		Effluent	20.0	–	0.06	9.0	0.89	0.7

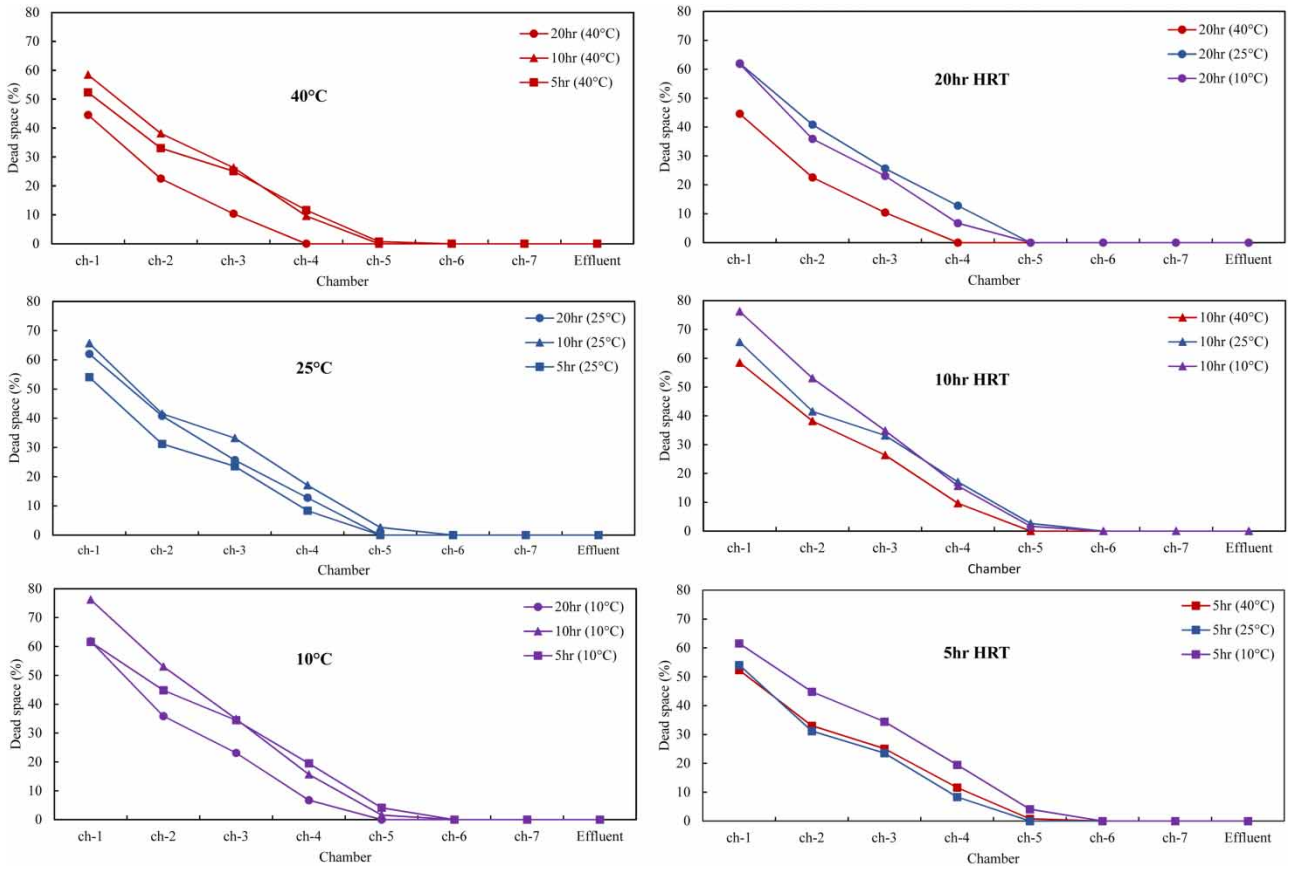

Figure 3 | Dead space of chambers (1–effluent) of the HABR for different runs (A1–C3).

The dead space became zero at chamber 4 only at high HRT and temperature (20 hr and 40 °C). In addition, it became zero at chamber 5 either at high temperature (40 °C) with lower HRTs (5 hr or 10 hr) or at higher HRT (20 hr) with lower temperatures (10 °C or 25 °C), whereas it became zero at chamber 6 either at lower HRTs (5 hr or 10 hr) and/or lower temperatures (10 °C or 25 °C). This shows that the dead space is mainly influenced by number of chambers in the reactor than by HRTs and/or influent temperature. As the number of reactor chambers increases, the dead space in the reactor gradually decreases. Hydraulic dead space tends to occur due to stagnant eddies forming under weirs and in corners of the reactor. The eddies effectively act as reservoirs, into and out of which the tracer slowly diffuses. On the C-curve, this appears as a smooth tail: the larger the hydraulic dead space, the greater is the area of the tail (Liu *et al.* 2007).

As mentioned earlier, short circuiting is a complicated phenomenon resulting from inadequate mixing, poor design, density currents and channelling effect within the reactor. Thus, it affects the reactor hydraulic performance by producing a dead zone (Tsai *et al.* 2012). The short circuiting during all runs was calculated using Equation (7) as presented in Table 3. The results showed that there were short circuiting (value less than or equal to 0.3) effects up to chamber 3 or 4, which might be due to density current and channelling effect on the front chambers. There were minimum effects observed in short circuiting due to variation of HRTs and feed temperatures. Overall, the results revealed that a reactor (similar HABR configuration) with six chambers would reduce the hydraulic dead space to zero with no short circuiting effect under different HRTs (5, 10, and 20 hr) and feed temperatures (10, 25, and 40 °C).

Mixing patterns and hydraulic model

Flow pattern refers to the mixing of materials, which has a considerable bearing on the performance of the reactor, and can be described by the dispersion index, namely dispersion numbers D_d (Sharma & Kazmi 2015). The dispersion index and the mean residence time are entirely independent of one another. A reactor with high mean residence time (C_θ peak close to $\theta = 1$) but high dispersion

index would have lower solids removal efficiencies or treatment efficiencies (Thackston *et al.* 1987). While designing the reactor, it is required to have higher mean residence time and ideal intermediate dispersion, which will ultimately increase the system treatment efficiency.

By using the AD model Equation (10), the dispersion numbers of the system were calculated as presented in Table 3. The results showed that the dispersion numbers for chamber 1 varied between 0.43 and ∞ (i.e. high value) indicating a perfectly mixed system as a CSTR for all experimental runs. The dispersion numbers for chamber 2 and 3 were between 0.28 and 0.52 and between 0.19 and 0.33, respectively, which indicated large degree of dispersion ($\infty \geq D_d \geq 0.2$) except for 0.18 and 0.13 in chamber 2 and 3, respectively, at 20 hr HRT and 25 °C feed temperature. The dispersion number varied between 0.04 and 0.18 from chamber 4 to effluent sample indicating intermediate dispersion ($0.2 \geq D_d \geq 0.02$) between completely mixed and plug-flow system, which was an ideal condition for an effective treatment performance, for all experimental runs. Figure 4(a) shows that the effects of variable HRTs and influent temperature were mainly observed up to chamber 4 for all runs. There was no influence of dispersion numbers observed in the floated filter media chamber 6 and 7, since there was no adsorption effect of tracer materials on the filter media. The ideal intermediate dispersion ($0.2 \geq D_d \geq 0.02$) was achieved from chamber 5 to effluent for all runs. Xu *et al.* (2014) also had similar finding of negative correlation between the degree of back-mixing and the number of chambers in the reactor. The fluid in the reactor gradually approached the plug-flow state with the increasing number of chambers in the reactor.

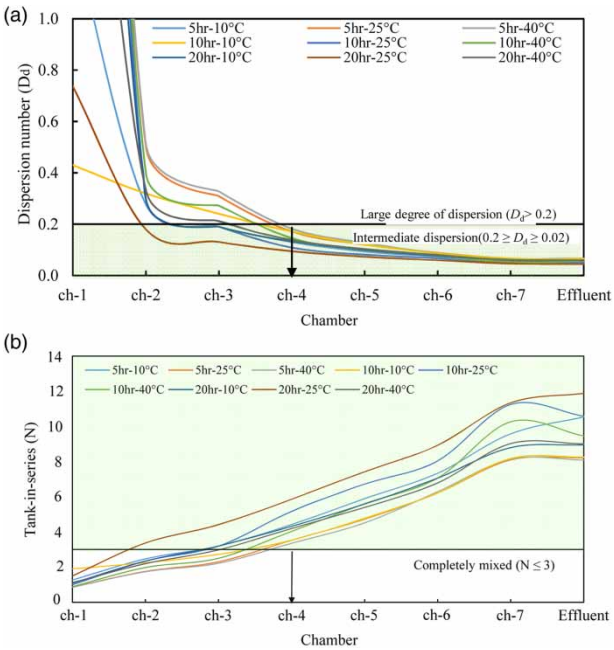

Figure 4 | (a) Dispersion number of chambers (1–effluent) of the HABR for different runs (A1–C3). (b) TIS (N) of chambers (1–effluent) of the HABR for different runs (A1–C3).

In the TIS model, the mixing pattern is characterized by N, which can be obtained from the reciprocal of the dimensionless variance from the E-curve. At $N \leq 3$ the flow is considered as completely mixed (Ji *et al.* 2012). The back-mixing predicted by TIS model was similar to the back-mixing predicted by AD model. The TIS model, which was based on the dimensionless variance, indicated that the first three chambers of the reactor behaved as a CSTR ($N \leq 3$) for all runs as shown in Figure 4(b). The N varied between 3.4 and 11.9 from chamber 4 to effluent sample indicating intermediate dispersion condition between completely mixed ($N = 1$) and plug-flow system ($N = \infty$) for all runs A1 to C3. Table 3 shows the results, where the values of N exceeded the number of actual chambers. The interpretation of this phenomenon was that the baffles in the reactor inhibited back-mixing between chambers; however, significant mixing within each individual chamber was observed (Li *et al.* 2016).

Reactor hydraulic efficiency

According to Equation (15), the hydraulic efficiency is related to both the effective volume and the flow pattern; hence on the one hand, it is related to the pollutant removal efficiency of the system, and on the other hand, it is influenced by hydraulic characteristics (Ji *et al.* 2012). Thus, the hydraulic efficiency represents the ability of the system to distribute its flow uniformly throughout its volume, maximizing the contact time of pollutant in the system, and optimizing the ability to break down the pollutants. It is classified as excellent hydraulic efficiency when $\lambda > 0.75$, good hydraulic efficiency when $0.5 < \lambda \leq 0.75$, and poor hydraulic efficiency when $\lambda \leq 0.5$. The hydraulic efficiencies of the HABR were calculated for all different runs A1 to C3 as shown in Table 3 and Figure 5.

The hydraulic efficiencies for the first two chambers were below 0.42 indicating poor efficiencies ($\lambda \leq 0.5$) for all runs. In different feed temperatures between 10 °C and 40 °C, the chamber 3 showed good hydraulic efficiency (0.53 to 0.60) at higher HRTs (i.e. 20 hr), but dropped to poor efficiency (0.41 to 0.46) at lower HRTs (i.e. 5 hr or 10 hr). In addition, the chamber 4 showed excellent efficiency of 0.76 at higher 20 hr HRT and good efficiency

between 0.60 and 0.72 at lower 5 hr or 10 hr HRT for different feed temperature. Excellent hydraulic efficiencies from 0.77 to 0.92 were achieved in chamber 5 through to effluent for all conditions.

Statistical analysis

In order to find the relationship between the variables (HRT, feed temperature, reactor's chamber) and the hydrodynamic responses (V_d, Pe and λ), a full factorial design analysis was conducted using RSM. The RSM provides useful second order (quadratic) and third order (cubic) relationships between the variables and responses. A general form of the quadratic equation can be expressed as following:

$$Y = b_0 + \sum_{i=1}^{n} b_i X_i + \sum_{i=1}^{n} b_{ii} X_i^2 + \sum_{i=1}^{n} \sum_{j>1}^{n} b_{ij} X_i X_j \qquad (16)$$

where Y is the response; b_0 is the constant coefficient; b_i, b_{ii}, and b_{ij} are the linear, quadratic, and interaction coefficients; and X_i and X_j are the coded values of the independent variables, respectively (Sahu *et al.* 2009; Nazari *et al.* 2017). In this study, 72 experimental data obtained from all nine runs (A1 to C3) were analysed by RSM. Each factor was coded at three levels between −1 and +1, whereas the independent factors were HRT = 5–20 hr, influent temperature = 10–40 °C, and chamber = 1–8 (as effluent).

One quadratic model for each response was developed for the data fitting in order to quantify the curvature effects for responses: dead space, Peclet number, and hydraulic efficiency (Table 4). The analysis of variance (ANOVA) results for the relevant responses are also summarized in Table 4. Since the amount of R-squared (R^2) and adjusted R-squared (adj. R^2) between experimental and model predicted were near to each other and close to 1.0, the fit of the models was verified. Adequate precision (AP ≥ 4) for all responses was demonstrated by the range measurement of the predicted response relative to its associated error (Pirsaheb *et al.* 2015). F-test was applied to assess the adequacy of correlations. The lack of fit F-statistic was not statistically

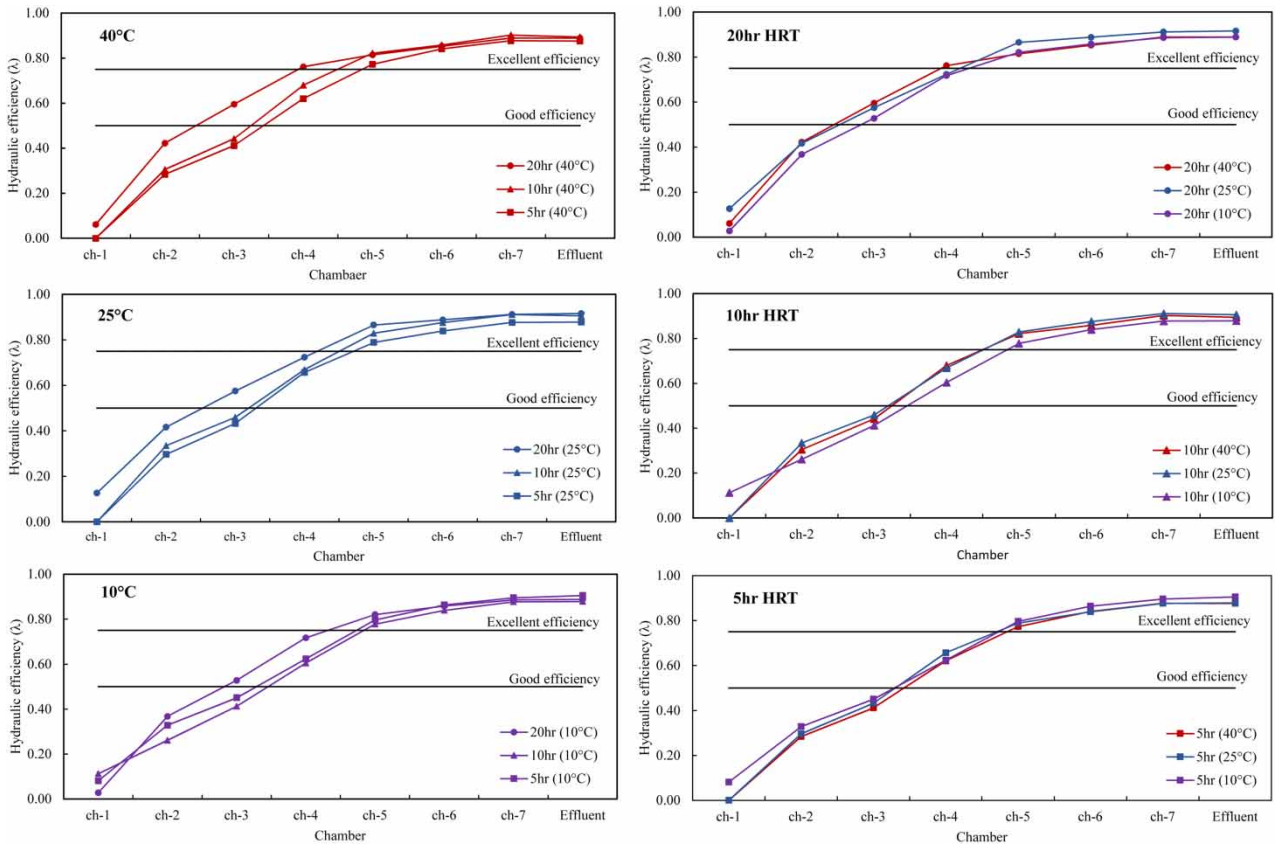

Figure 5 | Hydraulic efficiency of chambers (1–effluent) of the HABR for different runs (A1–C3).

Table 4 | ANOVA results for the equations and correlation values from the response surface methodology

Response	Type of model	Modified equations with significant terms	F-value	*P*-value	R^2	Adj. R^2	Pred. R^2	CV %	AP
Dead space	Quadratic	$+10.39 - 1.21A - 2.95B - 28.82C - 0.23AB + 1.56AC + 4.28BC - 4.18A^2 - 0.63B^2 + 22.98C^2$	221.64	<0.0001	0.9699	0.9655	0.9592	23.72	48.97
Peclet number	Quadratic	$+10.51 + 0.90A - 0.23B + 9.28C + 0.43AB + 0.27*AC + 0.22BC - 0.51A^2 - 1.51B^2 + 0.63C^2$	107.80	<0.0001	0.9399	0.9312	0.6167	18.00	36.37
Hydraulic efficiency	Quadratic	$+0.74 + 0.028A + 4.003E - 003B + 0.408C + 0.012AB - 0.021AC + 5.787E - 004BC + 6.173E - 003A^2 - 0.017B^2 - 0.255C^2$	410.70	<0.0001	0.98446	0.9822	0.9772	5.28	67.17

Note: A – HRT (h), B – temperature (°C), C – chamber, CV – coefficient of variation.

significant owing to the low *P*-values (<0.0005) for all model equations.

Figure 6(a)–6(c) shows combined effects of HRT and influent temperature on dead space along the different chambers in the HABR. It appeared that the dead space was primarily influence by feed temperature rather than HRT in the first four chambers (1–4): high dead space observed at low temperature (10 °C) and vice versa. This temperature influence was minimized on the rear chambers (5–7), where the dead space was influenced by both HRT and temperature changes. It is also to be noted that the dead space is mainly influenced by number of chambers in the reactor. As the number of chambers increases, the dead space decreases.

As mentioned earlier, the flow patter is often characterized by *Pe* ($\mu L/D$). At $Pe \leq 5$, the flow is considered as intermediate mixing between large degree of dispersion and completely mixed (Li *et al.* 2015). It was found in this study that the mixing pattern (*Pe*) was significantly affected by the feed temperature: strong back-mixing observed in either low (10 °C) or high (40 °C) temperature, and weaker back-mixing observed at temperature close to 25 °C (Figure 6(d)–6(f)). However, *Pe* was found to be more than 5 (intermediate mixing between CSTR and plug flow) on rear chambers (4–7) for all runs. Similar effects were observed for hydraulic efficiencies at variable influent temperatures (10–40 °C); however, excellent hydraulic efficiency ($\lambda > 0.75$) was observed when HRT increased to 20 hr (Figure 6(g)–6(i)).

Nachaiyasit & Stuckey (1997) operated an eight-chamber ABR at variable temperatures (15, 25, and 35 °C), and reported that there was no or low effect on treatment efficiencies when temperature dropped from 35 °C to 25 °C, but treatment efficiencies declined when temperature dropped to 15 °C. Feng *et al.* (2008) also reported that the operational temperature had strong influence on effluent suspended solids (SS) (15 mg/L SS in effluent at 28 °C and 35–40 mg/L SS at 10 °C). In addition, Wu *et al.* (2016) operated a pilot-scale ABR and membrane bioreactor combined process for wastewater treatment for 301 days, and also reported that the process enabled a relatively stable and high removal performance under 25 ± 5 °C compared with 10 ± 5 °C and 35 ± 5 °C. Based on the Arrhenius relationship, a decrease in temperature results in a decrease in the reaction rate, and for a 10 °C drop, biological reaction rates are expected to drop by a half (Nachaiyasit & Stuckey 1997). However, the treatment efficiency of the ABR in the above studies was not dropped due to temperature variation from 35 °C to 25 °C. Perhaps, this was because of weaker back-mixing (intermediate dispersion between CSTR and plug flow) that existed in the ABR at temperature close to 25 °C as supported by the finding of this study.

Figure 6(j)–6(l) presents a good convergence between the actual and the predicted values for all responses (V_d, *Pe*, λ), suggesting that the actual values are distributed relatively close to the straight line (y = x). A reasonable agreement between R^2 values and adj. R^2 values for all responses (V_d, *Pe*, λ) (less than 0.02) indicates the good consistency between predicted and actual values of the RSM assessment.

Overall, the results indicate that the reactor performance is greatly influenced by the number of chambers in the reactor rather than HRT and influent temperature. The influence of HRT and feed temperature was mainly observed on the front (1–4) chambers rather than rear chambers (5–7). The optimum reactor performance – low dead space (<10%), excellent hydraulic efficiency ($\lambda > 0.75$), and intermediate mixing pattern ($Pe > 10$) – can be achieved using the proposed HABR with more than five chambers.

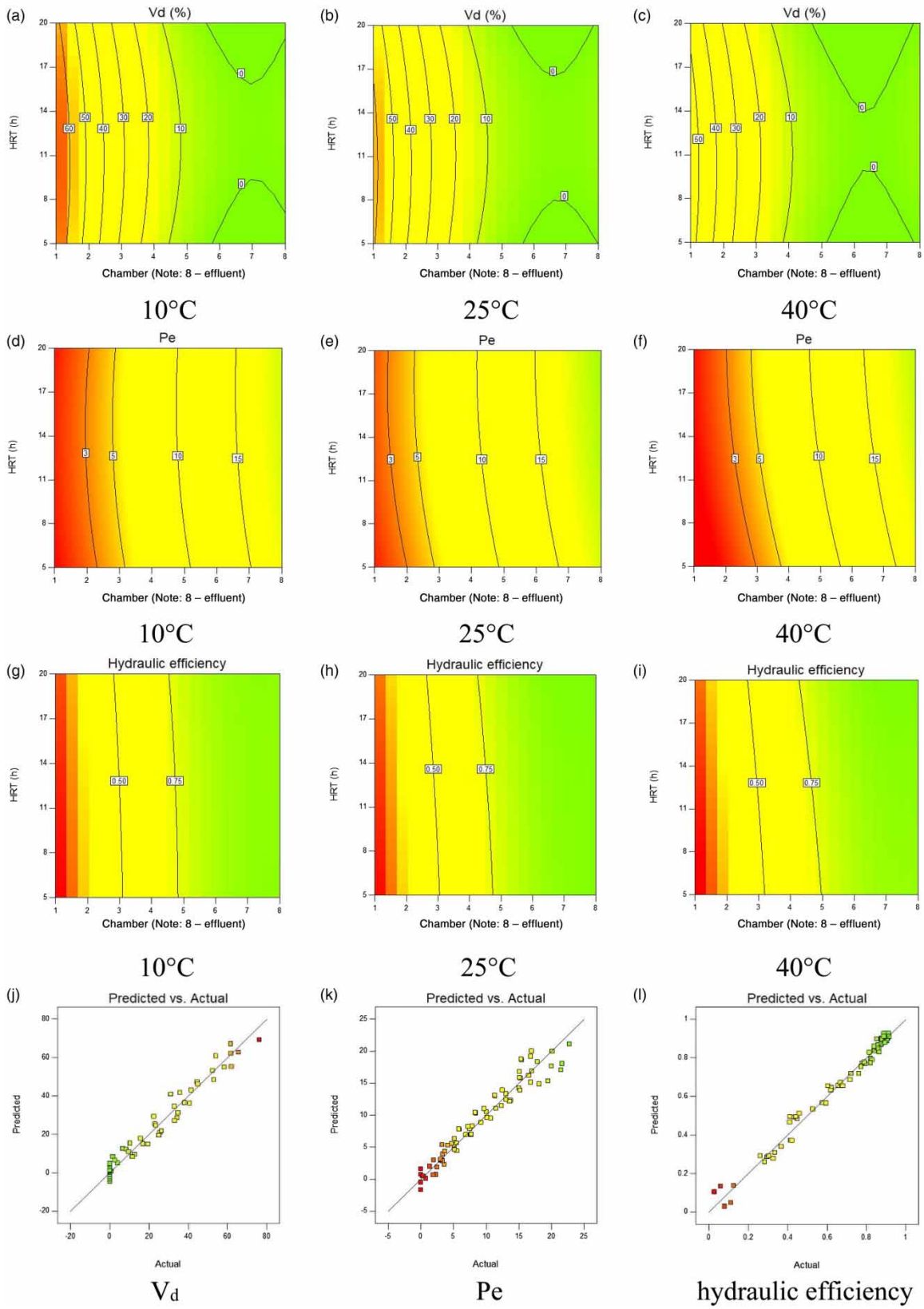

Figure 6 | Contour plots of the interactive effect for V_d (a–c), *Pe* (d–f), and hydraulic efficiency (g–i); actual vs predicted for V_d (j), *Pe* (k), and hydraulic efficiency (l).

CONCLUSION

A HABR was proposed with improved design principles, consisting of a front sedimentation chamber and four regular baffled chambers, followed by two floated filter media chambers. Tracer experiments were conducted for the RTD study in order to evaluate the effects of operating variables: 5–20 hr HRT, and 10–40 °C influent temperature. In addition, a full factorial design analysis was conducted using RSM to determine their interactive effects on the hydrodynamic responses: dead space, Peclet number, and hydraulic efficiency of the HABR. The study suggests that reactor hydraulic behaviour is primarily influenced by the number of chambers rather than HRT and influent temperature. The feed temperature and HRT mainly affects the front chambers (1–4) rather than rear chambers (5–7). The proposed HABR was found to achieve optimum reactor performance with more than five chambers.

ACKNOWLEDGEMENTS

The project was partially funded by University Grants Commission (UGC), Bangladesh, and Water Aid Bangladesh (WAB).

REFERENCES

Chan, Y. J., Chong, M. F., Law, C. L. & Hassell, D. G. 2009 A review on anaerobic–aerobic treatment of industrial and municipal wastewater. *Chem. Eng. J.* **155**, 1–18. https://doi.org/10.1016/j.cej.2009.06.041.

Feng, H., Hu, L., Mahmood, Q., Qiu, C., Fang, C. & Shen, D. 2008 Anaerobic domestic wastewater treatment with bamboo carrier anaerobic baffled reactor. *Int. Biodeterior. Biodegrad.* **62**, 232–238. https://doi.org/10.1016/j.ibiod.2008.01.009.

Feng, H., Hu, L., Mahmood, Q., Fang, C., Qiu, C. & Shen, D. 2009 Effects of temperature and feed strength on a carrier anaerobic baffled reactor treating dilute wastewater. *Desalination* **239**, 111–121. https://doi.org/10.1016/j.desal.2008.03.011.

Grobicki, A. & Stuckey, D. C. 1992 Hydrodynamic characteristics of the anaerobic baffled reactor. *Water Res.* **26**, 371–378.

Ji, J., Zheng, K., Xing, Y. & Zheng, P. 2012 Hydraulic characteristics and their effects on working performance of compartmentalized anaerobic reactor. *Bioresour. Technol.* **116**, 47–52. https://doi.org/10.1016/j.biortech.2012.04.026.

Levenspiel, O. 1999 *Chemical Reaction Engineering*, 3rd edn. Wiley, New York.

Li, S., Nan, J., Li, H. & Yao, M. 2015 Comparative analyses of hydraulic characteristics between the different structures of two anaerobic baffled reactors (ABRs). *Ecol. Eng.* **82**, 138–144. https://doi.org/10.1016/j.ecoleng.2015.04.095.

Li, S., Nan, J. & Gao, F. 2016 Hydraulic characteristics and performance modeling of a modified anaerobic baffled reactor (MABR). *Chem. Eng. J.* **284**, 85–92. https://doi.org/10.1016/j.cej.2015.08.129.

Liew Abdullah, A. G., Idris, A., Ahmadun, F. R., Baharin, B. S., Emby, F., Megat Mohd Noor, M. J. & Nour, A. H. 2005 A kinetic study of a membrane anaerobic reactor (MAR) for treatment of sewage sludge. *Desalination* **183**, 439–445. https://doi.org/10.1016/j.desal.2005.03.044.

Liu, X., Ren, N. & Wan, C. 2007 Hydrodynamic characteristics of a four-compartment periodic anaerobic baffled reactor. *J. Environ. Sci.* **19**, 1159–1165. https://doi.org/10.1016/S1001-0742(07)60189-2.

Metcalf & Eddy 2003 *Wastewater Engineering: Treatment and Reuse*, 4th edn. McGraw-Hill Education, New York.

Nachaiyasit, S. & Stuckey, D. C. 1997 Effect of low temperatures on the performance of an anaerobic baffled reactor (ABR). *J. Chem. Technol. Biotechnol.* **69**, 276–284. https://doi.org/10.1002/(SICI)1097-4660(199706)69:2<276::AID-JCTB711 > 3.0.CO;2-T.

Nazari, L., Yuan, Z., Ray, M. B. & Xu, C. (Charles) 2017 Co-conversion of waste activated sludge and sawdust through hydrothermal liquefaction: optimization of reaction parameters using response surface methodology. *Appl. Energy* **203**, 1–10. https://doi.org/10.1016/j.apenergy.2017.06.009.

Persson, J., Somes, N. L. G. & Wong, T. H. F. 1999 Hydraulics efficiency of constructed wetlands and ponds. *Water Sci. Technol.* **40**, 291–300. https://doi.org/10.1016/S0273-1223(99)00448-5.

Pirsaheb, M., Rostamifar, M., Mansouri, A. M., Zinatizadeh, A. A. L. & Sharafi, K. 2015 Performance of an anaerobic baffled reactor (ABR) treating high strength baker's yeast manufacturing wastewater. *J. Taiwan Inst. Chem. Eng.* **47**, 137–148. https://doi.org/10.1016/j.jtice.2014.09.029.

Qi, W.-K., Hojo, T. & Li, Y.-Y. 2013 Hydraulic characteristics simulation of an innovative self-agitation anaerobic baffled reactor (SA-ABR). *Bioresour. Technol.* **136**, 94–101. https://doi.org/10.1016/j.biortech.2013.02.033.

Renuka, R., Mariraj Mohan, S. & Amal Raj, S. 2016 Hydrodynamic behaviour and its effects on the treatment performance of panelled anaerobic baffle-cum filter reactor. *Int. J. Environ. Sci. Technol.* **13**, 307–318. https://doi.org/10.1007/s13762-015-0824-z.

Reynaud, N. & Buckley, C. A. 2016 The anaerobic baffled reactor (ABR) treating communal wastewater under mesophilic conditions: a review. *Water Sci. Technol.* **73**, 463–478. https://doi.org/10.2166/wst.2015.539.

Sahu, J. N., Acharya, J. & Meikap, B. C. 2009 Response surface modeling and optimization of chromium(VI) removal from aqueous solution using Tamarind wood activated carbon in batch process. *J. Hazard. Mater.* **172**, 818–825. https://doi.org/10.1016/j.jhazmat.2009.07.075.

Sarathai, Y., Koottatep, T. & Morel, A. 2010 Hydraulic characteristics of an anaerobic baffled reactor as onsite wastewater treatment system. *J. Environ. Sci.* **22**, 1319–1326. https://doi.org/10.1016/S1001-0742(09)60257-6.

Sharma, M. K. & Kazmi, A. A. 2015 Effect of physical property of supporting media and variable hydraulic loading on hydraulic characteristics of advanced onsite wastewater treatment system. *Environ. Technol.* **36**, 1414–1422. https://doi.org/10.1080/09593330.2014.992480.

Thackston, E. L., Shields, F. D. & Schroeder, P. R. 1987 Residence time distributions of shallow basins. *J. Environ. Eng.* **113**, 1319–1332. https://doi.org/10.1061/(ASCE)0733-9372(1987)113:6(1319).

Tsai, D. D.-W., Ramaraj, R. & Chen, P. H. 2012 A method of short-circuiting comparison. *Water Resour. Manag.* **26**, 2689–2702. https://doi.org/10.1007/s11269-012-0040-2.

Wu, P., Peng, Q., Xu, L., Wang, J., Huang, Z., Zhang, J. & Shen, Y. 2016 Effects of temperature on nutrient removal performance of a pilot-scale ABR/MBR combined process for raw wastewater treatment. *Desalination Water Treat.* **57**, 12074–12081. https://doi.org/10.1080/19443994.2015.1048741.

Xu, M., Ding, L., Xu, K., Geng, J. & Ren, H. 2014 Flow patterns and optimization of compartments for the anaerobic baffled reactor. *Desalination Water Treat.* 1–8. https://doi.org/10.1080/19443994.2014.970580.

First received 21 February 2018; accepted in revised form 17 August 2018. Available online 29 August 2018